Importance of Isobar Density Distributions on the Chiral Magnetic Effect Search

Hao-jie Xu,[1] Xiaobao Wang,[1] Hanlin Li,[2] Jie Zhao,[3] Zi-Wei Lin,[4,5] Caiwan Shen,[1] and Fuqiang Wang[1,3,*]

[1]School of Science, Huzhou University, Huzhou, Zhejiang 313000, China
[2]College of Science, Wuhan University of Science and Technology, Wuhan, Hubei 430065, China
[3]Department of Physics and Astronomy, Purdue University, West Lafayette, Indiana 47907, USA
[4]Department of Physics, East Carolina University, Greenville, North Carolina 27858, USA
[5]Key Laboratory of Quarks and Lepton Physics (MOE) and Institute of Particle Physics, Central China Normal University, Wuhan, Hubei 430079, China

(Received 7 March 2018; revised manuscript received 7 May 2018; published 11 July 2018)

Under the approximate chiral symmetry restoration, quark interactions with topological gluon fields in quantum chromodynamics can induce a chirality imbalance and parity violation in local domains. An electric charge separation (CS) could be generated along the direction of a strong magnetic field (**B**), a phenomenon called the chiral magnetic effect (CME). CS measurements by azimuthal correlators are contaminated by major backgrounds from elliptic flow anisotropy (v_2). Isobaric $^{96}_{44}\mathrm{Ru}+{}^{96}_{44}\mathrm{Ru}$ and $^{96}_{40}\mathrm{Zr}+{}^{96}_{40}\mathrm{Zr}$ collisions have been proposed to identify the CME (expected to differ between the two systems) out of the backgrounds (to be almost the same). We show, by using the density functional theory calculations of the proton and neutron distributions, that these expectations may not hold as originally anticipated because the two systems may have sizable differences in eccentricity and v_2.

DOI: 10.1103/PhysRevLett.121.022301

Introduction.—Because of vacuum fluctuations, topological gluon fields can emerge in quantum chromodynamics (QCD) [1]. The interactions of quarks with those gluon fields can induce chirality imbalance and parity violation in local domains under the approximate chiral symmetry restoration [1–4], likely achieved in relativistic heavy ion collisions (HICs) at BNL's Relativistic Heavy Ion Collider (RHIC) [5–8] and CERN's Large Hadron Collider (LHC) [9]. A chirality imbalance could lead to an electric current, or charge separation (CS), in the direction of a strong magnetic field (**B**) [4]. This phenomenon is called the chiral magnetic effect (CME) [10]. Searching for the CME is one of the most active areas of research in HICs [11–19]. The CME is not specific to QCD, but is a macroscopic phenomenon generally arising from quantum anomalies [20]. It is a subject of interest for a wide range of physics communities; such phenomena have been observed in magnetized relativistic matter in three-dimensional Dirac and Weyl materials [21–23].

In HICs, the CS is commonly measured by the three-point correlator [24], $\gamma \equiv \cos(\phi_\alpha + \phi_\beta - 2\psi_{\mathrm{RP}})$, where ϕ_α and ϕ_β are the azimuthal angles of two charged particles, and ψ_{RP} is that of the reaction plane (RP, spanned by the impact parameter and beam directions) to which the **B** produced by the incoming protons is perpendicular on average [25–28]. Often a third particle azimuthal angle is used in place of ψ_{RP} with a resolution correction [11,12]. Because of charge-independent backgrounds, such as correlations from global momentum conservation, the correlator difference between opposite-sign (OS) and same-sign (SS) pairs, $\Delta\gamma \equiv \gamma_{\mathrm{OS}} - \gamma_{\mathrm{SS}}$, is used. Positive $\Delta\gamma$ signals, consistent with the CME-induced CS perpendicular to the RP, have been observed [11–15]. The signals are, however, inconclusive because of a large charge-dependent background arising from particle correlations (e.g., resonance decays) coupled with the elliptic flow anisotropy (v_2) [29–31]. Take $\rho^0 \to \pi^+\pi^-$ as an example [24,32]. Because of the v_2 of ρ, more OS pairs align in the RP than **B** direction, leading to a sizable signal: $\Delta\gamma \propto \langle \cos(\alpha + \beta - 2\phi_\rho)\cos 2(\phi_\rho - \psi_{\mathrm{RP}})\rangle \propto v_{2,\rho}$ [32]. In other words, the γ_{OS} variable is ambiguous between a CME-induced back-to-back pair (CS) perpendicular to the RP and a resonance-decay pair (charge alignment) along the RP [16,29,30].

There have been many attempts to reduce or eliminate the v_2-induced backgrounds [16,32–35]. STAR [16] found a charge asymmetry signal to linearly depend on the event-by-event v_2 of final-state particles, suggesting a background dominance. CMS [18] and ALICE [19] divided their data from each collision centrality according to their event-by-event v_2 and found the $\Delta\gamma$ signal to be proportional to v_2, consistent with a null CME.

To better control the background, isobaric collisions of $^{96}_{44}\mathrm{Ru}+{}^{96}_{44}\mathrm{Ru}$ (RuRu) and $^{96}_{40}\mathrm{Zr}+{}^{96}_{40}\mathrm{Zr}$ (ZrZr) have been proposed [36]. One expects their backgrounds to be almost equal because of the same mass number, while the atomic numbers, hence **B**, differ by 10%. This is verified by Monte Carlo–Glauber (MCG) calculations [37] using the Woods-Saxon (WS) density profile,

$$\rho_{\rm WS}(r,\theta) \propto (1+\exp[\{r-R_0[1+\beta_2 Y_2^0(\theta)]\}/a])^{-1}, \quad (1)$$

where $R_0 = 5.085$ and 5.020 fm are used for Ru and Zr, respectively, $a = 0.46$ fm, and Y_2^0 is a spherical harmonic. The deformity quadrupole parameter β_2 has large uncertainties; current knowledge suggests two contradicting sets of values [37], 0.158 (Ru) and 0.080 (Zr) [38,39] *vis-à-vis* 0.053 (Ru) and 0.217 (Zr) [40–42]. This would yield a less than ±2% difference in eccentricity (ϵ_2), hence a residual v_2 background, between RuRu and ZrZr collisions in the 20%–60% centrality range [37]. $\mathbf{B}^2$, to which the CME strength in $\Delta\gamma$ is proportional, differs by approximately 15% (not the simple 19% because of the slightly smaller R_0 value used for Zr than Ru) [37]. As a net result, the CME signal-to-background ratio would be improved by over a factor of 7 in comparative measurements between RuRu and ZrZr collisions than in each of them individually [37]. The isobaric collisions are planned for 2018 at the RHIC; they would yield a CME signal of 5σ significance with the projected data volume, if one assumes that the CME contributes 1/3 of the current $\Delta\gamma$ measurement in AuAu collisions [37].

However, there can be non-negligible deviations of the Ru and Zr nuclear densities from WS. The purpose of this Letter is to investigate those deviations and their effects on the sensitivity of isobaric collisions for the CME search.

Nuclear densities.—Because of the different numbers of protons—which suffer from Coulomb repulsion—and neutrons, the structures of the $^{96}_{44}$Ru and $^{96}_{40}$Zr nuclei must not be identical. Measurements of their charge and mass densities are, however, scarce [37–39]. Their knowledge requires theoretical calculations [40–43]. Much of the theoretical understanding of proton and neutron distributions in nuclei have come, so far, from density functional theory (DFT) [44,45]. While *ab initio* methods have been employed to calculate nuclear structures up to ^{48}Ca [46,47], DFT is at present the only microscopic approach that can be applied throughout the entire nuclear chart [48]. It employs energy density functionals that incorporate complex many-body correlations into functionals that are primarily constrained by global nuclear properties, such as binding energies and radii [44–46]. By using DFT, we calculate the Ru and Zr proton and neutron distributions using the well-known SLy4 mean field [49], including pairing correlations [Hartree-Fock-Bogoliubov (HFB) approach] [43,44,50,51]. The calculated ground-state proton and nucleon (proton + neutron) densities, assumed spherical, are shown in Fig. 1. Protons in Zr are more concentrated in the core, while protons in Ru, 10% more than in Zr, are pushed more toward outer regions. The neutrons in Zr, four more than in Ru, are more concentrated in the core, but also more populated on the nuclear skin.

Theoretical uncertainties are estimated by using different sets of density functionals, SLy5 [49] and SkM* [52] for the mean field, with and without pairing (HFB/HF) [44,50,51], and found to be small. The deformities of Ru and Zr are uncertain, allowed by a wide range of possibilities [37–42]. Our DFT calculations indicate that their ground states are soft against deformation and can be nearly spherical. Their densities are calculated with the allowed extreme values of β_2 (0.158 for Ru and 0.217 for Zr [38–42]). They yield the largest uncertainties on our results.

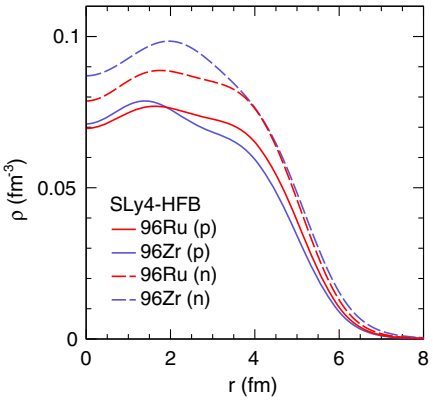

FIG. 1. Proton and neutron density distributions of the $^{96}_{44}$Ru and $^{96}_{40}$Zr nuclei, assumed spherical, calculated by the DFT method.

Eccentricity and magnetic field.—The ϵ_2 of the transverse overlap geometry in RuRu and ZrZr collisions is calculated event by event with MCG [53–57], using the nucleon densities in Fig. 1, by

$$\epsilon_2\{\psi_{\rm PP}\}_{\rm evt} e^{i2\psi_{\rm PP}} = \langle r_\perp^2 e^{i2\phi_r}\rangle / \langle r_\perp^2\rangle. \quad (2)$$

Here $\langle\ldots\rangle$ denotes the per-event average; $(r_\perp,\phi_r)$ is the polar coordinate of each initial participant nucleon in the transverse plane, whose origin $\mathbf{r} = 0$ is taken to be the center of mass of all participant nucleons. The ϵ_2 is the average over many events, $\epsilon_2\{\psi_{\rm PP}\} \equiv \langle \epsilon_2\{\psi_{\rm PP}\}_{\rm evt}\rangle$. The nucleon-nucleon cross section is taken to be 42 mb [56,58] with the "Gaussian" approach [55]; a minimum nucleon-nucleon separation of 0.4 fm is required [56,58]. Uncertainties on these values have a negligible effect on our results. The $\epsilon_2\{\psi_{\rm PP}\}$ is the eccentricity with respect to the participant plane (PP). Because of the finite number effect, the PP azimuthal angle $\psi_{\rm PP}$ fluctuates about the RP azimuthal angle, $\psi_{\rm RP}$ (fixed at 0) [53]; the ϵ_2 of the averaged overlap geometry is

$$\epsilon_2\{\psi_{\rm RP}\} = \langle \epsilon_2\{\psi_{\rm PP}\}\cos 2(\psi_{\rm PP}-\psi_{\rm RP})\rangle. \quad (3)$$

The $\epsilon_2\{\psi_{\rm PP}\}$ and $\epsilon_2\{\psi_{\rm RP}\}$ calculated using the DFT densities are shown in Fig. 2(a) as functions of the impact parameter (b).

$\mathbf{B}(\mathbf{r}, t = 0)$ is calculated for RuRu and ZrZr collisions using the proton densities in Fig. 1. The calculations follow Refs. [27,59], with a finite proton radius (0.88 fm [59] is used but the numeric value is not critical) to avoid the singularity at zero relative distance. The relevant quantity [37] for the CME strength in a $\Delta\gamma$ measurement, with

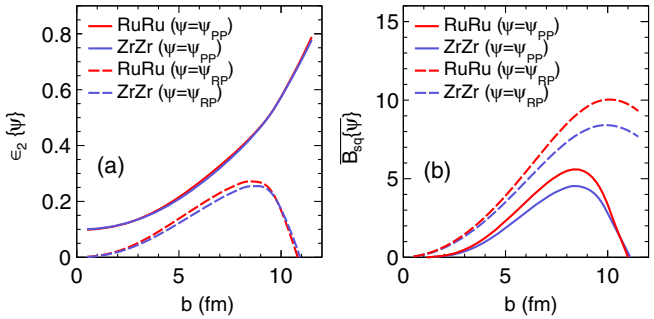

FIG. 2. (a) $\epsilon_2\{\psi\}$ and (b) $\overline{B_{\rm sq}}\{\psi\}$ with respect to $\psi=\psi_{\rm RP}$ and $\psi_{\rm PP}$ as functions of b in RuRu and ZrZr collisions, calculated by MCG with the DFT densities in Fig. 1.

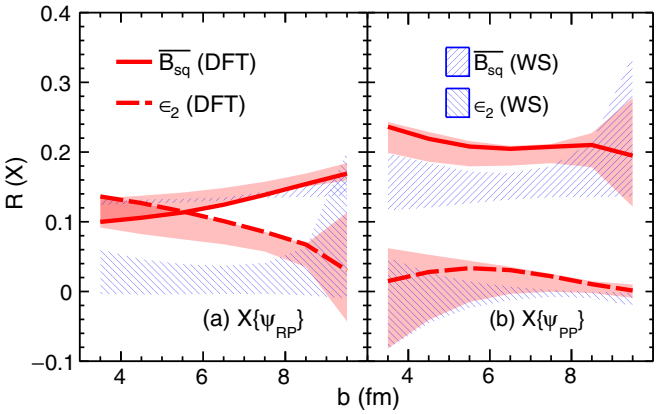

FIG. 3. Relative differences between RuRu and ZrZr collisions in $\epsilon_2\{\psi\}$ and $\overline{B_{\rm sq}}\{\psi\}$ with respect to (a) $\psi=\psi_{\rm RP}$ and (b) $\psi=\psi_{\rm PP}$, using the DFT densities in Fig. 1. The shaded areas correspond to DFT density uncertainties from Ru and Zr deformities; the hatched areas show the corresponding results using WS of Eq. (1).

respect to an azimuth ψ, is the event average $\overline{B_{\rm sq}}\{\psi\}\equiv\langle\overline{B_{\rm sq}}\{\psi\}_{\rm evt}\rangle$,

$$\overline{B_{\rm sq}}\{\psi\}_{\rm evt}\equiv\int N_{\rm part}^2(\mathbf{r})(eB(\mathbf{r},0)/m_\pi^2)^2\cos 2(\psi_{\rm B}-\psi)d\mathbf{r}\Big/\int N_{\rm part}^2(\mathbf{r})d\mathbf{r},\tag{4}$$

where $N_{\rm part}(\mathbf{r})$ is the transverse density of participant nucleons. The average is weighted by $N_{\rm part}^2$ because $\Delta\gamma$ is a pairwise observable; our results are, however, only weakly sensitive to the $N_{\rm part}$-weighting power. Figure 2(b) shows $\overline{B_{\rm sq}}\{\psi_{\rm RP}\}$ and $\overline{B_{\rm sq}}\{\psi_{\rm PP}\}$ calculated using the DFT densities. Since $\mathbf{B}$ in noncentral HICs comes primarily from the spectator protons, its event-averaged direction is perpendicular to $\psi_{\rm RP}$, not $\psi_{\rm PP}$. $\overline{B_{\rm sq}}\{\psi_{\rm PP}\}$ is a projection of and hence always smaller than $\overline{B_{\rm sq}}\{\psi_{\rm RP}\}$, in contrast to the case for ϵ_2 in Eq. (3).

For the CME search with isobaric collisions, the relative differences in ϵ_2 and $\overline{B_{\rm sq}}$ are of importance. Figure 3 shows the relative differences $R(\epsilon_2\{\psi_{\rm PP}\})$, $R(\epsilon_2\{\psi_{\rm RP}\})$, $R(\overline{B_{\rm sq}}\{\psi_{\rm PP}\})$, and $R(\overline{B_{\rm sq}}\{\psi_{\rm RP}\})$; $R(X)$ is defined as [37]

$$R(X)\equiv 2(X_{\rm RuRu}-X_{\rm ZrZr})/(X_{\rm RuRu}+X_{\rm ZrZr}),\tag{5}$$

where $X_{\rm RuRu}$ and $X_{\rm ZrZr}$ are the X values in RuRu and ZrZr collisions, respectively. The thick solid curves are the default results with the DFT densities in Fig. 1. The shaded areas correspond to theoretical uncertainties bracketed by the two DFT density cases, where Ru is deformed with $\beta_2=0.158$ and Zr is spherical, and where Ru is spherical and Zr is deformed with $\beta_2=0.217$. The hatched areas represent our results using WS densities in Eq. (1) with the above two cases of nuclear deformities.

Event plane and elliptic anisotropy.—We investigate whether our density profiles would, in a dynamical model, lead to a final-state v_2 difference between RuRu and ZrZr collisions and whether the $\overline{B_{\rm sq}}$ difference preserves with respect to the event plane (EP) reconstructed from the final-state particle momenta. We employ a multiphase transport (AMPT) model with "string melting" [60,61], which can reasonably reproduce heavy ion bulk data at the RHIC and the LHC [62,63]. The initial condition of AMPT is taken from HIJING [64]. We implement our DFT nuclear densities into the HIJING component in AMPT. The string-melting AMPT converts the HIJING-produced initial hadrons into their valence quarks [60,61], which further evolve via two-body elastic scatterings [65]. The Debye-screened differential cross section $d\sigma/dt\propto\alpha_s^2/(t-\mu_D^2)^2$ [61] is used, with strong coupling constant $\alpha_s=0.33$ and screening mass $\mu_D=2.265/\text{fm}$ (so the total cross section is $\sigma=3$ mb). After quarks stop interacting, a simple coalescence model is applied to describe the hadronization process that converts quarks into hadrons [61]. We switch off subsequent hadronic scatterings in AMPT, as was done in Refs. [35,66]; while responsible for the majority of the v_2 mass splitting, they are not important for the v_2 magnitude [67,68].

The multiphase transport version and parameter values used in the present Letter are the same as those used earlier for RHIC collisions in [62,63,67–69]. A total on the order of 5×10^6 minimum-bias events each is simulated for RuRu and ZrZr collisions with b from 0 to 12 fm. The charged particle (hereafter referring to $\pi^\pm$, $K^\pm$, p, and $\bar{p}$ within pseudorapidity $|\eta|<1$) multiplicity ($N_{\rm ch}$) distribution in RuRu has a slightly higher tail than that in ZrZr. The difference is insignificant; for example, the 20%–60% centrality corresponds to the $N_{\rm ch}$ range of 62–273 and 61–271 in RuRu and ZrZr, respectively.

The EP azimuthal angle is reconstructed similar to Eq. (2), $v_2\{\psi_{\rm EP}^{\rm rec}\}_{\rm evt}e^{i2\psi_{\rm EP}^{\rm rec}}=\langle e^{i2\phi}\rangle$, but with final-state charged particle azimuthal angle ϕ in momentum space. The v_2 is corrected by the EP resolution ($\mathcal{R}_{\rm EP}$), $v_2\{\psi_{\rm EP}\}=\langle v_2\{\psi_{\rm EP}^{\rm rec}\}_{\rm evt}\rangle/\mathcal{R}_{\rm EP}$ [70]. The v_2 with respect to the RP is

simply given by $v_2\{\psi_{\rm RP}\} = \langle\cos 2(\phi - \psi_{\rm RP})\rangle$, where $\psi_{\rm RP} = 0$ is fixed. The $v_2\{\psi_{\rm RP}\}$ and $v_2\{\psi_{\rm EP}\}$ are found to follow the b dependence of the eccentricities calculated in AMPT (which are consistent with those from our MCG). $\mathbf{B}(\mathbf{r}, t = 0)$ is also computed from the initial incoming protons in AMPT, as done in MCG, for $\overline{B_{\rm sq}}\{\psi_{\rm RP}\}$ and $\overline{B_{\rm sq}}\{\psi_{\rm EP}\} \equiv \overline{B_{\rm sq}}\{\psi_{\rm EP}^{\rm rec}\}/\mathcal{R}_{\rm EP}$. $\overline{B_{\rm sq}}\{\psi_{\rm RP}\}$ is consistent with that calculated by MCG; $\overline{B_{\rm sq}}\{\psi_{\rm EP}\}$ is found to be similar to $\overline{B_{\rm sq}}\{\psi_{\rm PP}\}$. Figure 4 shows $R(v_2\{\psi_{\rm RP}\})$, $R(v_2\{\psi_{\rm EP}\})$, $R(\overline{B_{\rm sq}}\{\psi_{\rm RP}\})$, and $R(\overline{B_{\rm sq}}\{\psi_{\rm EP}\})$ from AMPT as functions of centrality, determined from the $N_{\rm ch}$ distributions. The general trends are similar to those in Fig. 3.

Discussions and Summary.—Isobaric RuRu and ZrZr collisions were proposed to help search for the CME for their expected different $\mathbf{B}$ and equal ϵ_2 [36]. These expectations are qualitatively verified by MCG calculations using WS in Eq. (1) [37]. We have generally reproduced those results with our MCG, which are shown as the hatched areas in Fig. 3. Our $\overline{B_{\rm sq}}$ is an average over the transverse overlap area, while in Ref. [37] it is that at ($\mathbf{0}$, 0). The RuRu-ZrZr differences in these two $\overline{B_{\rm sq}}$ quantities are less similar for our DFT calculated densities than for the more regular WS.

$R(\overline{B_{\rm sq}}\{\psi_{\rm RP}\})$ is slightly smaller for the DFT density profiles than for WS at small b. This is consistent with the hierarchy in the charge radii differences between Ru and Zr: $\sqrt{\langle r^2\rangle} = 4.327$ and 4.271 fm from DFT and those from Eq. (1). The Zr mass radius (4.366 fm from DFT) is, on the other hand, not smaller than Ru's (4.343 fm), making the $N_{\rm ch}$ distribution tail in RuRu slightly higher than in ZrZr, opposite to that in Ref. [37]. For CS measurements with respect to the second order harmonic EP, however, it is the $\overline{B_{\rm sq}}\{\psi_{\rm PP}\}$, not the $\overline{B_{\rm sq}}\{\psi_{\rm RP}\}$, that matters. $R(\overline{B_{\rm sq}}\{\psi_{\rm PP}\})$ from the DFT densities is larger than its WS counterpart. It is interesting to note that $R(\overline{B_{\rm sq}}\{\psi_{\rm PP}\})$ is always larger than $R(\overline{B_{\rm sq}}\{\psi_{\rm RP}\})$; it is found to arise from a better alignment of $\psi_{\rm PP}$ with $\psi_{\rm RP}$ in RuRu, by about 10%, than in ZrZr. This is because the Ru mass density outweighs the Zr's in the outer region, while Zr is more concentrated at the core, making the $\psi_{\rm PP}$ better determined in RuRu than in ZrZr.

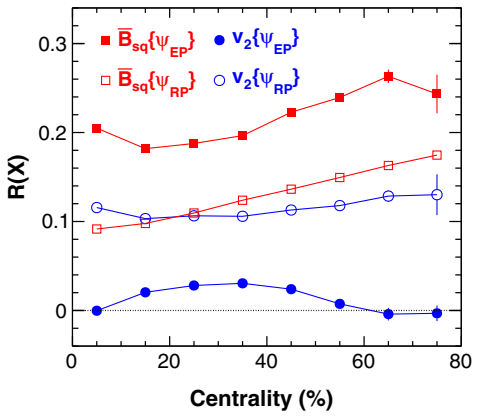

FIG. 4. Relative differences between RuRu and ZrZr collisions as functions of centrality in $v_2\{\psi\}$ (of charged particles in $|\eta| < 1$) and $\overline{B_{\rm sq}}\{\psi\}$ with respect to $\psi = \psi_{\rm RP}$ and $\psi_{\rm EP}$, simulated by AMPT with the DFT densities in Fig. 1.

The DFT calculated densities introduce a large $\epsilon_2\{\psi_{\rm RP}\}$ difference, as large as that in $\overline{B_{\rm sq}}\{\psi_{\rm RP}\}$. This means that, with respect to RP, the premise of isobaric collisions to help identify the CME does not hold. The DFT calculated densities introduce a sizable $\epsilon_2\{\psi_{\rm PP}\}$ difference, up to $R(\epsilon_2\{\psi_{\rm PP}\}) \approx 3.7\%$ at $b \approx 5$ fm [Fig. 3(b), dashed curves], and an average v_2 difference $R(v_2\{\psi_{\rm EP}\}) \approx 2.7 \pm 0.1\%$ in 20%–60% centrality (Fig. 4, filled circles). Although this v_2 difference is significantly smaller than the difference in the magnetic field, it can have a sizable effect on the isobar difference because of the background dominance in the experimental $\Delta\gamma$ measurement. For example, suppose 10% of the measured $\Delta\gamma$ comes from the CME signal, then the $\overline{B_{\rm sq}}$ difference of 20% would introduce only a 2% effect, while the v_2 difference gives a 2.4% effect. In other words, one could measure a 4.4% isobar difference in $\Delta\gamma$, out of which more than half is due to background. The sizable $\epsilon_2\{\psi_{\rm PP}\}$ and $v_2\{\psi_{\rm EP}\}$ difference weakens the power of isobaric collisions to search for the CME. A direct calculation of the γ correlators with realistic backgrounds and an assumed CME signal would be valuable to the CME search. Experimentally the v_2 will be measured, which would gauge what the geometry difference is likely to be between RuRu and ZrZr. Our work suggests that a sizable v_2 difference up to ~3% is likely and one needs to carefully examine v_2 and $\Delta\gamma$ measurements in assessing the possible CME signal.

In summary, topological charge fluctuations are a fundamental property of QCD, which could lead to the chiral magnetic effect and charge separation in relativistic heavy ion collisions. Experimental CS measurements have suffered from major backgrounds from resonance decays coupled with elliptic flow anisotropy v_2. To reduce background effects, isobaric ${}^{96}_{44}\mathrm{Ru} + {}^{96}_{44}\mathrm{Ru}$ and ${}^{96}_{40}\mathrm{Zr} + {}^{96}_{40}\mathrm{Zr}$ collisions have been proposed where the v_2-induced backgrounds are expected to be similar while the CME-induced signals are expected to be different. In this Letter, the proton and neutron density distributions of ${}^{96}_{44}\mathrm{Ru}$ and ${}^{96}_{40}\mathrm{Zr}$ are calculated using the energy density functional theory. They are then implemented in the Monte Carlo–Glauber model to calculate the eccentricities ϵ_2 and magnetic fields $\mathbf{B}$; the DFT densities are implemented in a multiphase transport model to simulate the v_2. It is found that those nuclear densities, together with the Woods-Saxon densities, yield wide ranges of differences in $\overline{B_{\rm sq}}$ with respect to the participant and reaction planes. It is further found that those nuclear densities introduce, in contrast to WS, comparable differences in $\epsilon_2\{\psi_{\rm RP}\}$ ($v_2\{\psi_{\rm RP}\}$) and $\overline{B_{\rm sq}}\{\psi_{\rm RP}\}$ with respect to the reaction plane, diminishing the premise of

isobaric collisions to help identify the CME. With respect to the participant plane, the $\epsilon_2\{\psi_{\mathrm{PP}}\}$ ($v_2\{\psi_{\mathrm{EP}}\}$) difference can still be sizable, as large as ~3%, possibly weakening the power of isobaric collisions for the CME search.

Since the DFT calculation of the matter radius is smaller for Ru and Zr, the produced particle multiplicity distribution would have a higher tail in RuRu than in ZrZr, as predicted by AMPT. This can be checked against results using density distributions of larger $^{96}_{44}$Ru than $^{96}_{40}$Zr radius, such as WS densities using charge radii in place of matter radii. We further predict, using the DFT calculated density distributions, that the v_2 difference between RuRu and ZrZr with respect to the RP is larger than that with respect to the PP by an absolute 8%, insensitive to uncertainties in the nuclear deformities, while it is practically zero for WS. This can be experimentally tested by the upcoming isobaric collisions; a confirmation would be a good indication of the validity of the density distributions calculated here for the Ru and Zr nuclei. Our study would then be a valuable guidance to the experimental isobaric collision program at the RHIC.

F. W. thanks B. Alex Brown for useful discussions. This work was supported in part by the National Natural Science Foundation of China under Grants No. 11647306, No. 11747312, No. U1732138, No. 11505056, No. 11605054, and No. 11628508 and U.S. Department of Energy Award No. DE-SC0012910.

*fqwang@zjhu.edu.cn

[1] T. Lee and G. Wick, Phys. Rev. D **9**, 2291 (1974).
[2] P. D. Morley and I. A. Schmidt, Z. Phys. C **26**, 627 (1985).
[3] D. Kharzeev, R. D. Pisarski, and M. H. G. Tytgat, Phys. Rev. Lett. **81**, 512 (1998).
[4] D. E. Kharzeev, L. D. McLerran, and H. J. Warringa, Nucl. Phys. **A803**, 227 (2008).
[5] I. Arsene *et al.* (BRAHMS Collaboration), Nucl. Phys. **A757**, 1 (2005).
[6] B. Back *et al.* (PHOBOS Collaboration), Nucl. Phys. **A757**, 28 (2005).
[7] J. Adams *et al.* (STAR Collaboration), Nucl. Phys. **A757**, 102 (2005).
[8] K. Adcox *et al.* (PHENIX Collaboration), Nucl. Phys. **A757**, 184 (2005).
[9] B. Muller, J. Schukraft, and B. Wyslouch, Annu. Rev. Nucl. Part. Sci. **62**, 361 (2012).
[10] K. Fukushima, D. E. Kharzeev, and H. J. Warringa, Phys. Rev. D **78**, 074033 (2008).
[11] B. Abelev *et al.* (STAR Collaboration), Phys. Rev. Lett. **103**, 251601 (2009).
[12] B. Abelev *et al.* (STAR Collaboration), Phys. Rev. C **81**, 054908 (2010).
[13] B. Abelev *et al.* (ALICE Collaboration), Phys. Rev. Lett. **110**, 012301 (2013).
[14] L. Adamczyk *et al.* (STAR Collaboration), Phys. Rev. C **88**, 064911 (2013).
[15] L. Adamczyk *et al.* (STAR Collaboration), Phys. Rev. Lett. **113**, 052302 (2014).
[16] L. Adamczyk *et al.* (STAR Collaboration), Phys. Rev. C **89**, 044908 (2014).
[17] V. Khachatryan *et al.* (CMS Collaboration), Phys. Rev. Lett. **118**, 122301 (2017).
[18] A. M. Sirunyan *et al.* (CMS), Phys. Rev. C **97**, 044912 (2018).
[19] S. Acharya *et al.* (ALICE), Phys. Lett. B **777**, 151 (2018).
[20] D. E. Kharzeev, J. Liao, S. A. Voloshin, and G. Wang, Prog. Part. Nucl. Phys. **88**, 1 (2016).
[21] Q. Li, D. E. Kharzeev, C. Zhang, Y. Huang, I. Pletikosic, A. V. Fedorov, R. D. Zhong, J. A. Schneeloch, G. D. Gu, and T. Valla, Nat. Phys. **12**, 550 (2016).
[22] B. Q. Lv *et al.*, Phys. Rev. X **5**, 031013 (2015).
[23] X. Huang *et al.*, Phys. Rev. X **5**, 031023 (2015).
[24] S. A. Voloshin, Phys. Rev. C **70**, 057901 (2004).
[25] D. Kharzeev, Phys. Lett. B **633**, 260 (2006).
[26] A. Bzdak and V. Skokov, Phys. Lett. B **710**, 171 (2012).
[27] W.-T. Deng and X.-G. Huang, Phys. Rev. C **85**, 044907 (2012).
[28] J. Bloczynski, X.-G. Huang, X. Zhang, and J. Liao, Phys. Lett. B **718**, 1529 (2013).
[29] F. Wang, Phys. Rev. C **81**, 064902 (2010).
[30] A. Bzdak, V. Koch, and J. Liao, Phys. Rev. C **81**, 031901 (2010).
[31] S. Schlichting and S. Pratt, Phys. Rev. C **83**, 014913 (2011).
[32] F. Wang and J. Zhao, Phys. Rev. C **95**, 051901 (2017).
[33] N. N. Ajitanand, R. A. Lacey, A. Taranenko, and J. M. Alexander, Phys. Rev. C **83**, 011901 (2011).
[34] A. Bzdak, Phys. Rev. C **85**, 044919 (2012).
[35] J. Zhao, H. Li, and F. Wang, arXiv:1705.05410.
[36] S. A. Voloshin, Phys. Rev. Lett. **105**, 172301 (2010).
[37] W.-T. Deng, X.-G. Huang, G.-L. Ma, and G. Wang, Phys. Rev. C **94**, 041901 (2016).
[38] S. Raman, C. W. G. Nestor, Jr., and P. Tikkanen, At. Data Nucl. Data Tables **78**, 1 (2001).
[39] B. Pritychenko, M. Birch, B. Singh, and M. Horoi, At. Data Nucl. Data Tables **107**, 1 (2016).
[40] P. Moller, J. R. Nix, W. D. Myers, and W. J. Swiatecki, At. Data Nucl. Data Tables **59**, 185 (1995).
[41] B. Kumar, S. K. Singh, and S. K. Patra, Int. J. Mod. Phys. E **24**, 1550017 (2015).
[42] P. Moller, A. J. Sierk, T. Ichikawa, and H. Sagawa, At. Data Nucl. Data Tables **109–110**, 1 (2016).
[43] X. B. Wang, J. L. Friar, and A. C. Hayes, Phys. Rev. C **94**, 034314 (2016).
[44] M. Bender, P.-H. Heenen, and P.-G. Reinhard, Rev. Mod. Phys. **75**, 121 (2003).
[45] J. Erler, N. Birge, M. Kortelainen, W. Nazarewicz, E. Olsen, A. M. Perhac, and M. Stoitsov, Nature (London) **486**, 509 (2012).
[46] G. Hagen *et al.*, Nat. Phys. **12**, 186 (2015).
[47] R. F. Garcia Ruiz *et al.*, Nat. Phys. **12**, 594 (2016).
[48] M. Kortelainen, J. Phys. G **42**, 034021 (2015).
[49] E. Chabanat, P. Bonche, P. Haensel, J. Meyer, and R. Schaeffer, Nucl. Phys. **A635**, 231 (1998); **A643**, 441(E) (1998).
[50] R. M. Dreizler and E. K. U. Gross, *Density Functional Theory: An Approach to the Quantum Many-Body Problem* (Springer, Berlin, 1990).

[51] P. Ring and P. Schuck, *The Nuclear Many-body Problem*, Texts and Monographs in Physics (Springer, New York, 2000).
[52] J. Bartel, P. Quentin, M. Brack, C. Guet, and H. B. Hakansson, Nucl. Phys. **A386**, 79 (1982).
[53] B. Alver *et al.* (PHOBOS Collaboration), Phys. Rev. Lett. **98**, 242302 (2007).
[54] M. L. Miller, K. Reygers, S. J. Sanders, and P. Steinberg, Annu. Rev. Nucl. Part. Sci. **57**, 205 (2007).
[55] M. Rybczynski and W. Broniowski, Phys. Rev. C **84**, 064913 (2011).
[56] H. J. Xu, Q. Wang, and L. Pang, Phys. Rev. C **89**, 064902 (2014).
[57] X. Zhu, Y. Zhou, H. Xu, and H. Song, Phys. Rev. C **95**, 044902 (2017).
[58] B. Abelev *et al.* (STAR Collaboration), Phys. Rev. C **79**, 034909 (2009).
[59] W.-T. Deng and X.-G. Huang, Phys. Lett. B **742**, 296 (2015).
[60] Z.-W. Lin and C. M. Ko, Phys. Rev. C **65**, 034904 (2002).
[61] Z.-W. Lin, C. M. Ko, B.-A. Li, B. Zhang, and S. Pal, Phys. Rev. C **72**, 064901 (2005).
[62] Z.-W. Lin, Phys. Rev. C **90**, 014904 (2014).
[63] G.-L. Ma and Z.-W. Lin, Phys. Rev. C **93**, 054911 (2016).
[64] X.-N. Wang and M. Gyulassy, Phys. Rev. D **44**, 3501 (1991).
[65] B. Zhang, Comput. Phys. Commun. **109**, 193 (1998).
[66] G.-L. Ma and B. Zhang, Phys. Lett. B **700**, 39 (2011).
[67] H. Li, L. He, Z.-W. Lin, D. Molnar, F. Wang, and W. Xie, Phys. Rev. C **93**, 051901 (2016).
[68] H. Li, L. He, Z.-W. Lin, D. Molnar, F. Wang, and W. Xie, Phys. Rev. C **96**, 014901 (2017).
[69] L. He, T. Edmonds, Z.-W. Lin, F. Liu, D. Molnar, and F. Wang, Phys. Lett. B **753**, 506 (2016).
[70] A. M. Poskanzer and S. A. Voloshin, Phys. Rev. C **58**, 1671 (1998).